Chapter 6

Molecular Dynamics in Various Ensembles

The Molecular Dynamics technique discussed in Chapter 4 is a scheme for studying the natural time evolution of a classical system of N particles in volume V. In such simulations, the total energy E is a constant of motion. If we assume that time averages are equivalent to ensemble averages, then the (time) averages obtained in a conventional MD simulation are equivalent to ensemble averages in the microcanonical (constant-NVE) ensemble. However, as was discussed in Chapter 5, it is often more convenient to perform simulations in other ensembles (e.g., N,V,T or N,P,T). At first sight, it would seem that it is impossible to perform MD simulations in ensembles other than the microcanonical. Fortunately, it turns out that this is not the case. Two rather different solutions to this problem have been proposed. One is based on the idea that dynamical simulation of other ensembles is possible by mixing Newtonian MD with certain Monte Carlo moves. The second approach is completely dynamical in origin: it is based on a reformulation of the Lagrangian equations of motion of the system.

Both approaches occur time and again in many areas of MD simulation, and we will not attempt to list them all. In particular, the extended Lagrangian method, first introduced by Andersen in the context of constant-pressure MD simulations [104], has become one of the most important tricks to extend the applicability of MD simulations. To name but a few of the more conspicuous examples, the method is used in the Parrinello-Rahman scheme to simulate crystalline solids under conditions of constant stress [102, 103]. In this approach, both the volume and the shape of the crystal unit cell are allowed to fluctuate. As a consequence, the Parrinello-Rahman scheme is particularly useful for studying displacive phase transitions in solids.

In this chapter, we do not attempt to give a comprehensive, or even historical, presentation of non-NVE MD simulations. Rather, we have selected a single (but important) case that will be discussed in detail, namely, constant temperature simulations. This example allows us to illustrate the main features of the different approaches. The extension of this method to constant-pressure and -temperature simulations is discussed in less detail. With this background, the relevant literature on other applications of these Molecular Dynamics methods should be more accessible to the reader.

6.1 Molecular Dynamics at Constant Temperature

Before considering different schemes to perform Molecular Dynamics simulations at constant temperature, we should first specify what we mean by constant temperature. From a statistical mechanical point of view, there is no ambiguity: we can impose a temperature on a system by bringing it into thermal contact with a large heat bath (see section 2.1). Under those conditions, the probability of finding the system in a given energy state is given by the Boltzmann distribution and, for a classical system, the Maxwell-Boltzmann velocity distribution follows:

$$\mathcal{P}(p) = \left(\frac{\beta}{2\pi m}\right)^{3/2} \exp\left[-\beta p^2/(2m)\right]. \tag{6.1.1}$$

In particular, we then obtain the simple relation between the imposed temperature T and the (translational) kinetic energy per particle:

$$k_B T = m \langle v_\alpha^2 \rangle,$$

where m is the mass of the particle and v_α is the αth component of its velocity. As discussed in Chapter 4, this relation is often used to measure the temperature in a (microcanonical) MD simulation. However, the condition of constant temperature is not equivalent to the condition that the kinetic energy per particle is constant. To see this, consider the relative variance of the kinetic energy per particle in a canonical ensemble. If we constrain the kinetic energy to be always equal to its average, then the variance vanishes by construction. Now consider a system that is in thermal equilibrium with a bath. The relative variance in the kinetic energy of any given particle is simply related to the second and fourth moments of the Maxwell-Boltzmann distribution. For the second moment, $p^2 = \sum_\alpha p_\alpha^2$, we have

$$\langle p^2 \rangle = \int d\mathbf{p}\, p^2 \mathcal{P}(p) = \frac{3m}{\beta}$$

and for the fourth moment, $p^4 = \left(\sum_\alpha p_\alpha^2\right)^2$, we can write

$$\langle p^4 \rangle = \int d\mathbf{p}\, p^4 \mathcal{P}(p) = 15 \left(\frac{m}{\beta}\right)^2.$$

The relative variance of the kinetic energy of that particle is

$$\frac{\sigma_{p^2}^2}{\langle p^2 \rangle^2} \equiv \frac{\langle p^4 \rangle - \langle p^2 \rangle^2}{\langle p^2 \rangle^2} = \frac{15(m/\beta)^2 - (3m/\beta)^2}{(3m/\beta)^2} = \frac{2}{3}.$$

If we would use the kinetic energy per particle as a measure of the instantaneous temperature, then we would find that, in a canonical ensemble, this temperature (denoted by T_k) fluctuates. Its relative variance is

$$
\begin{aligned}
\frac{\sigma_{T_k}^2}{\langle T_k \rangle_{NVT}^2} &\equiv \frac{\langle T_k^2 \rangle_{NVT} - \langle T_k \rangle_{NVT}^2}{\langle T_k \rangle_{NVT}^2} \\
&= \frac{N\langle p^4 \rangle + N(N-1)\langle p^2 \rangle \langle p^2 \rangle - N^2 \langle p^2 \rangle^2}{N^2 \langle p^2 \rangle^2} \\
&= \frac{1}{N} \frac{\langle p^4 \rangle - \langle p^2 \rangle^2}{\langle p^2 \rangle^2} = \frac{2}{3N}.
\end{aligned}
$$

So indeed, in a canonical ensemble of a finite system, the instantaneous kinetic temperature T_k fluctuates. In fact, if we were to keep the average kinetic energy per particle rigorously constant, as is done in the so-called isokinetic MD scheme [29] or the more naive velocity-scaling schemes, then we would not simulate the true constant-temperature ensemble. In practice, the difference between isokinetic and canonical schemes is often negligible. But problems can be expected if isokinetic simulations are used to measure equilibrium averages that are sensitive to fluctuations. Moreover, one should distinguish between the isokinetic scheme of [29] and other, more or less ad hoc velocity-scaling methods. The isokinetic scheme of Evans and Morriss is well behaved in the sense that it yields the correct canonical ensemble averages for all properties that depend only on the positions of the particles [29, 126].

The ad hoc methods yield only the desired kinetic energy per particle but otherwise do not correspond to any known ensemble. Of course, any kind of temperature regulation, no matter how unphysical, can be used while preparing the system at a desired temperature (i.e., during equilibration). But, as efficient MD schemes exist that do generate a true canonical distribution, there is little need to use more suspect techniques to fix the temperature. Here we discuss two of the most widely used canonical MD schemes.

6.1.1 The Andersen Thermostat

In the constant-temperature method proposed by Andersen [104] the system is coupled to a heat bath that imposes the desired temperature. The coupling to a heat bath is represented by stochastic impulsive forces that act occasionally on randomly selected particles. These stochastic collisions with the heat

bath can be considered as Monte Carlo moves that transport the system from one constant-energy shell to another. Between stochastic collisions, the system evolves at constant energy according to the normal Newtonian laws of motion. The stochastic collisions ensure that all accessible constant-energy shells are visited according to their Boltzmann weight.

Before starting such a constant-temperature simulation, we should first select the strength of the coupling to the heat bath. This coupling strength is determined by the frequency of stochastic collisions. Let us denote this frequency by ν. If successive collisions are uncorrelated, then the distribution of time intervals between two successive stochastic collisions, $P(t;\nu)$, is of the Poisson form [127, 128]

$$P(t;\nu) = \nu \exp[-\nu t]. \tag{6.1.2}$$

where $P(t;\nu)dt$ is the probability that the next collision will take place in the interval $[t, t + dt]$.

A constant-temperature simulation now consists of the following steps:

1. Start with an initial set of positions and momenta $\{r^N(0), p^N(0)\}$ and integrate the equations of motion for a time Δt.

2. A number of particles are selected to undergo a collision with the heat bath. The probability that a particle is selected in a time step of length Δt is $\nu\Delta t$.

3. If particle i has been selected to undergo a collision, its new velocity will be drawn from a Maxwell-Boltzmann distribution corresponding to the desired temperature T. All other particles are unaffected by this collision.

The mixing of Newtonian dynamics with stochastic collisions turns the Molecular Dynamics simulation into a Markov process [47]. As shown in [104], a canonical distribution in phase space is invariant under repeated application of the Andersen algorithm. Combined with the fact that the Markov chain is also irreducible and aperiodic [104,127,128], this implies that the Andersen algorithm does, indeed, generate a canonical distribution. In Algorithms 14 and 15, we show how the Andersen method can be implemented in a Molecular Dynamics simulation.

Case Study 10 (Lennard-Jones: Andersen Thermostat)
In the present case study, we illustrate some of the strong and weak points of the Andersen thermostat. The first, and most important, thing to show is that this thermostat does produce a canonical distribution. Unfortunately, we can show this only indirectly: we can check whether the Andersen thermostat reproduces known properties of a canonical ensemble. In Figure 6.1 we compare the velocity distribution of a Lennard-Jones fluid as generated by the

Algorithm 14 (Molecular Dynamics: Andersen Thermostat)

```
program md_Andersen                    MD at constant temperature
call init(temp)                        initialization
call force(f,en)                       determine the forces
t=0
do while (t.lt.tmax)                   MD loop
    call integrate(1,f,en,temp)        first part of the eqs. of motion
    call force(f,en)                   determine the forces
    call integrate(2,f,en,temp)        second part of eqs. of motion
    t=t+dt
    call sample                        sample averages
enddo
stop
end
```

Comments to this algorithm:

1. *This part of the algorithm is very similar to the simple Molecular Dynamics program (Algorithm 3). The difference is that we use the velocity Verlet algorithm (see section 4.3) for the integration of the equations of motion:*

$$\begin{aligned}
r(t + \Delta t) &= r(t) + v(t)\Delta t + \frac{f(t)}{2m}\Delta t^2 \\
v(t + \Delta t) &= v(t) + \frac{f(t + \Delta t) + f(t)}{2m}\Delta t.
\end{aligned}$$

This algorithm is implemented in two steps, in step 1, `call integrate(1,f,en,temp)`*, we know the forces and velocities at time* t*, and we update* $r(t)$ *and determine*

$$v' = v(t) + \frac{f(t)}{2m}\Delta t.$$

Then, in `call force(f,en)` *we determine the forces at* $t+\Delta t$*; and finally we determine in step 2,* `call integrate(2,f,en,temp)`*, the velocities at time* $t + \Delta t$*,*

$$v(t + \Delta t) = v' + \frac{f(t + \Delta t)}{2m}\Delta t.$$

*The subroutine* `integrate` *is described in Algorithm 15.*

2. *Subroutines* `init` *and* `force` *are described in Algorithms 4 and 5, respectively. Subroutine* `sample` *is used to calculate ensemble averages.*

Algorithm 15 (Equations of Motion: Andersen Thermostat)

```
subroutine integrate(switch,f      integrate equations of motion:
                    ,en,temp)      with Andersen thermostat
if (switch.eq.1) then              first step velocity Verlet
   do i=1,npart
      x(i)=x(i)+dt*v(i)+           update positions current time
+        dt*dt*f(i)/2
      v(i)=v(i)+dt*f(i)/2          first update velocity
   enddo
else if (switch.eq.2) then         second step velocity Verlet
   tempa=0
   do i=1,npart
      v(i)=v(i)+dt*f(i)/2          second update velocity
      tempa=tempa+v(i)**2
   enddo
   tempa=tempa/(s*npart)           instantaneous temperature
   sigma=sqrt(temp)                Andersen heat bath
   do i=1,npart
      if (ranf().lt.nu*dt) then    test for collision with bath
         v(i)=gauss(sigma)         give particle Gaussian velocity
      endif
   enddo
endif
return
end
```

Comments to this algorithm:

1. *In this subroutine we use the velocity Verlet algorithm [69] (see notes to Algorithm 14).*

2. *The function* gauss(sigma) *returns a value taken from a Gaussian distribution with zero mean and standard deviation* sigma *(see Algorithm 44);* ranf() *is a uniform random number* $\in [0, 1]$.

3. *The collisions with the heat bath are Poisson distributed (6.1.2). The collision frequency* nu *is set at the beginning of the simulation.*

4. *In this algorithm, neither the total energy nor the total momentum is conserved.* s *depends on the mass of the particles* $s = 3/m$.
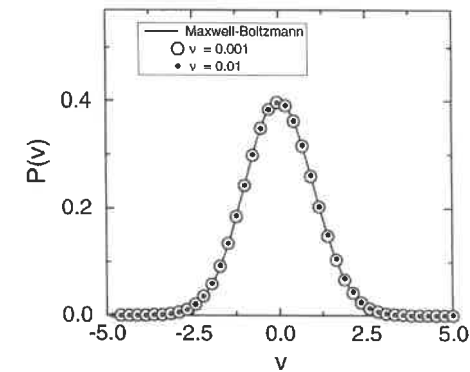
Figure 6.1: Velocity distribution in a Lennard-Jones fluid (T = 2.0, ρ = 0.8442, and N = 108). The solid line is the Maxwell-Boltzmann distribution (6.1.1), and the symbols are from a simulation using $\nu = 0.01$ and $\nu = 0.001$ as collision rates.

Andersen thermostat, with the exact Maxwell-Boltzmann distribution (6.1.1). The figure illustrates that the desired distribution is generated independent of the value of the collision frequency ν.

The results of constant N,V,T Molecular Dynamics simulations should be identical to those of canonical Monte Carlo simulations as presented in Figure 3.5. In making this comparison, we should be a bit careful because the Monte Carlo simulations were performed on a model with a truncated and shifted Lennard-Jones potential — the appropriate tail correction was added afterward. In our Molecular Dynamics program we simulate the Lennard-Jones model with a truncated and shifted potential. Again, the appropriate tail correction is added afterward (see section 3.2.2). For the Lennard-Jones fluid, the tail correction to the pressure is

$$P^{\text{tail}} = \frac{16}{3}\pi\rho^2\epsilon\sigma^6\left[\frac{2}{3}\left(\frac{\sigma}{r_c}\right)^9 - \left(\frac{\sigma}{r_c}\right)^3\right].$$

In Figure 6.2 the results of the Molecular Dynamics and Monte Carlo simulations are compared. In addition, we also compare them with the analytical equation-of-state data of [62]. Clearly, the canonical MD and MC simulations yield the same answer and agree with the equation-of-state data of [62]. This case study shows that the Andersen thermostat yields good results for time-independent properties, such as the equation of state. However, as the method is based on a stochastic scheme, one may wonder whether it can also be used to determine dynamic properties, such as the diffusion coeffi-
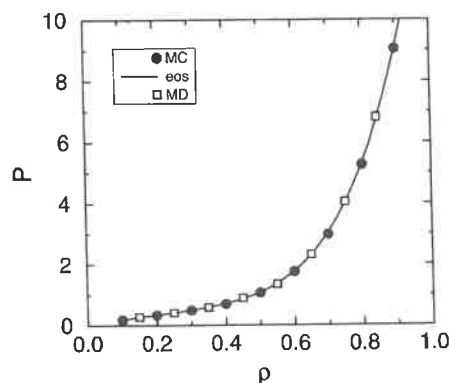
Figure 6.2: Equation of state of the Lennard-Jones fluid ($T = 2.0$ and $N = 108$); comparison of the Molecular Dynamics results using the Andersen thermostat (open symbols) with the results of Monte Carlo simulations (closed symbols) and the equation of state of Johnson *et al.* [62].

cient. In general, the answer to this question is no. The stochastic collisions disturb the dynamics in a way that is not realistic — it leads to sudden random decorrelation of particle velocities. This effect will result in an enhanced decay of the velocity autocorrelation function, and hence the diffusion constant (i.e., the time integral of the velocity autocorrelation function) is changed. Clearly this effect will be more pronounced as the collision frequency ν is increased. In fact, Tanaka *et al.* [129] have measured the diffusion coefficient of the Lennard-Jones fluid for various values of the collision frequency ν. They observed that the diffusion coefficient is independent of ν in a rather narrow frequency range. This effect is also illustrated in Figure 6.3. In practical cases, ν is usually chosen such that the decay rate of energy fluctuations in the simulation is comparable to that of energy fluctuations in a system of the same size embedded in an infinite heat bath. Typically, this can be achieved with relatively small collision rates and hence the effect of collisions on the dynamics may be small [104]. Nevertheless, one should always bear in mind that the dynamics generated by the Andersen thermostat is unphysical. It therefore is risky to use the Andersen method when studying dynamical properties. Figure 6.3 shows that the frequency of stochastic collisions has a strong effect on the time dependence of the mean-squared displacement. The mean-squared displacement becomes only independent of ν in the limit of very low stochastic collision rates. Yet, all static properties such as the pressure or potential energy are rigorously independent of the stochastic collision frequency.
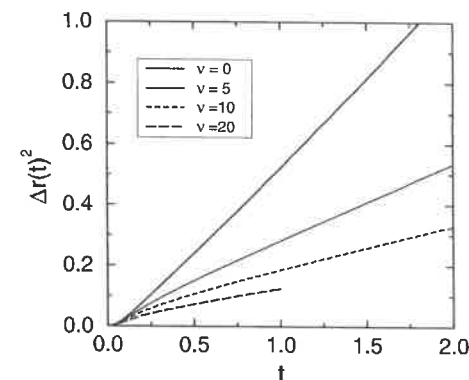
Figure 6.3: Mean-squared displacement as a function of time for various values of the collision frequency ν of the Lennard-Jones fluid ($T = 2.0$ and $N = 108$).

6.1.2 Nosé-Hoover Thermostat

In the Andersen approach to isothermal Molecular Dynamics simulation, constant temperature is achieved by stochastic collisions with a heat bath. Nosé has shown that one also can perform deterministic Molecular Dynamics at constant temperature [126, 130]. The approach of Nosé is based on the clever use of an extended Lagrangian; that is, a Lagrangian that contains additional, artificial coordinates and velocities. The extended-Lagrangian approach was introduced by Andersen [104] in the context of constant-pressure MD simulations. However, at present, extended Lagrangian methods are widely used not only for simulations in ensembles other than constant NVE, but also as a stable and efficient approach to perform simulations in which an expensive optimization has to be carried out at each time step. We discuss the Nosé thermostat as an illustration of an extended-Lagrangian method. However, for constant-temperature MD simulations, it is now more common to use the Nosé scheme in the formulation of Hoover [131, 132]. We therefore also discuss the so-called Nosé-Hoover thermostat.

In this section we assume that the reader is familiar with the Lagrangian and Hamiltonian formulation of classical mechanics. In Appendix A a review of these concepts is given.

Extended-Lagrangian Formulation

To construct isothermal Molecular Dynamics, Nosé introduced an additional coordinate s in the Lagrangian of a classical N-body system:

$$\mathcal{L}_{\text{Nose}} = \sum_{i=1}^{N} \frac{m_i}{2} s^2 \dot{\mathbf{r}}_i^2 - \mathcal{U}(\mathbf{r}^N) + \frac{Q}{2} \dot{s}^2 - \frac{L}{\beta} \ln s, \qquad (6.1.3)$$

where L is a parameter that will be fixed later. Q is an effective "mass" associated to s. The momenta conjugate to $\mathbf{r}_i$ and s follow directly from equation (6.1.3):

$$\mathbf{p}_i \equiv \frac{\partial \mathcal{L}}{\partial \dot{\mathbf{r}}_i} = m_i s^2 \dot{\mathbf{r}}_i \qquad (6.1.4)$$

$$p_s \equiv \frac{\partial \mathcal{L}}{\partial \dot{s}} = Q \dot{s}. \qquad (6.1.5)$$

This gives for the Hamiltonian of the extended system of the N particles plus additional coordinate s:

$$\mathcal{H}_{\text{Nose}} = \sum_{i=1}^{N} \frac{\mathbf{p}_i^2}{2 m_i s^2} + \mathcal{U}(\mathbf{r}^N) + \frac{p_s^2}{2Q} + L \frac{\ln s}{\beta}. \qquad (6.1.6)$$

We consider a system containing N atoms. The extended system generates a microcanonical ensemble of $6N + 2$ degrees of freedom. The partition function of this ensemble[1] is

$$
\begin{aligned}
Q_{\text{Nose}} &= \frac{1}{N!} \int dp_s ds dp^N dr^N \delta \left(E - \mathcal{H}_{\text{Nose}} \right) \\
&= \frac{1}{N!} \int dp_s ds dp'^N dr^N s^{3N} \\
&\quad \times \delta \left[\sum_{i=1}^{N} \frac{\mathbf{p'}_i^2}{2 m_i} + \mathcal{U}(\mathbf{r}^N) + \frac{p_s^2}{2Q} + \frac{L}{\beta} \ln s - E \right], \qquad (6.1.7)
\end{aligned}
$$

in which we have introduced

$$\mathbf{p}' = \mathbf{p}/s.$$

Let us define

$$\mathcal{H}(\mathbf{p}', \mathbf{r}) = \sum_{i=1}^{N} \frac{\mathbf{p'}_i^2}{2 m_i} + \mathcal{U}(\mathbf{r}^N). \qquad (6.1.8)$$

[1] We assume implicitly that conservation of energy is the only conservation law; in Appendix B.2 the more general case is considered.

For a δ function of a function $h(s)$, we can write

$$\delta[h(s)] = \delta(s - s_0)/|h'(s_0)|,$$

where $h(s)$ is a function that has a single root at s_0. If we substitute this expression into equation (6.1.7) and use equation (6.1.8), we find, for the partition function,

$$
\begin{aligned}
Q_{\text{Nose}} &= \frac{1}{N!} \int dp_s dp'^N dr^N ds \frac{\beta s^{3N+1}}{L} \\
&\quad \times \delta \left\{ s - \exp\left[-\beta \frac{\mathcal{H}(\mathbf{p}', \mathbf{r}) + p_s^2/(2Q) - E}{L} \right] \right\} \\
&= \frac{1}{N!} \frac{\beta \exp[E(3N+1)/L]}{L} \int dp_s \, \exp\left[-\beta \frac{3N+1}{L} p_s^2/(2Q) \right] \\
&\quad \times \int dp'^N dr^N \, \exp\left[-\beta \frac{3N+1}{L} \mathcal{H}(\mathbf{p}', \mathbf{r}) \right] \\
&= C \frac{1}{N!} \int dp'^N dr^N \, \exp\left[-\beta \frac{3N+1}{L} \mathcal{H}(\mathbf{p}', \mathbf{r}) \right]. \qquad (6.1.9)
\end{aligned}
$$

If we perform a simulation in this extended ensemble, the average of a quantity that depends on $\mathbf{p}', \mathbf{r}$ is given by

$$\bar{A} = \lim_{\tau \to \infty} \frac{1}{\tau} \int_0^\tau dt \, A(\mathbf{p}(t)/s(t), \mathbf{r}(t)) \equiv \langle A(\mathbf{p}/s, \mathbf{r}) \rangle_{\text{Nose}}. \qquad (6.1.10)$$

With the choice $L = 3N + 1$, this ensemble average reduces to the canonical average:

$$
\begin{aligned}
\langle A(\mathbf{p}/s, \mathbf{r}) \rangle_{\text{Nose}} &\equiv \frac{\int dp'^N dr^N A(\mathbf{p}', \mathbf{r}) \exp\left[-\beta \mathcal{H}(\mathbf{p}', \mathbf{r})(3N+1)/L \right]}{\int dp'^N dr^N \, \exp[-\beta \mathcal{H}(\mathbf{p}', \mathbf{r})(3N+1)/L]} \\
&= \frac{(1/N!) \int dp'^N dr^N A(\mathbf{p}', \mathbf{r}) \exp\left[-\beta \mathcal{H}(\mathbf{p}', \mathbf{r}) \right]}{Q(NVT)} \\
&= \langle A(\mathbf{p}', \mathbf{r}) \rangle_{\text{NVT}}. \qquad (6.1.11)
\end{aligned}
$$

It is instructive to consider the role of the variable s in some detail. In the ensemble average in equation (6.1.11), the phase space is spanned by the coordinates $\mathbf{r}$ and the scaled momenta $\mathbf{p}'$. As the scaled momentum is related most directly to observable properties, we refer to $\mathbf{p}'$ as the real momentum, while $\mathbf{p}$ is interpreted as a virtual momentum. We make a similar distinction between real and virtual for the other variables. Real variables are indicated by a prime, to distinguish them from their unprimed virtual counterparts.

The real and virtual variables are related as follows:

$$r' = r \qquad (6.1.12)$$
$$p' = p/s \qquad (6.1.13)$$
$$s' = {}'s \qquad (6.1.14)$$
$$\Delta t' = \Delta t/s. \qquad (6.1.15)$$

From equation (6.1.15) it follows that s can be interpreted as a scaling factor of the time step. This implies that the real time step fluctuates during a simulation. The sampling in equation (6.1.10) is done at integer multiples of the (virtual) time step Δt, which corresponds to real time steps that are not constant. It is also possible to sample at equal intervals in real time. In that case, we measure a slightly different average. Instead of equation (6.1.10) we define

$$\lim_{\tau' \to \infty} \frac{1}{\tau'} \int_0^{\tau'} dt' \, A\left[p(t')/s(t'), r(t')\right]. \qquad (6.1.16)$$

Equation (6.1.15) shows that the real and virtual measuring times τ' and τ, respectively, are related through

$$\tau' = \int_0^\tau dt \, 1/s(t).$$

This gives, for equation (6.1.16),

$$\lim_{\tau' \to \infty} \frac{1}{\tau'} \int_0^{\tau'} dt' \, A\left[p(t')/s(t'), r(t')\right]$$
$$= \lim_{\tau' \to \infty} \frac{\tau}{\tau'} \frac{1}{\tau} \int_0^\tau dt \, A\left[p(t)/s(t), r(t)\right]/s(t)$$
$$= \frac{\lim_{\tau \to \infty} \frac{1}{\tau} \int_0^\tau dt \, A\left[p(t)/s(t), r(t)\right]/s(t)}{\lim_{\tau \to \infty} \frac{1}{\tau} \int_0^\tau dt \, 1/s(t)}$$
$$= \langle A(p/s, r)/s \rangle / \langle 1/s \rangle. \qquad (6.1.17)$$

If we consider again the partition function (6.1.9), we can write for the ensemble average,

$$\frac{\langle A(p/s, r)/s \rangle}{\langle 1/s \rangle} \equiv \frac{\left\{ \dfrac{\int dp'^N dr^N \, A(p',r) \exp[-\beta \mathcal{H}(p',r)3N/L]}{\int dp'^N dr^N \, \exp[-\beta \mathcal{H}(p',r)3(N+1)/L]} \right\}}{\left\{ \dfrac{\int dp'^N dr^N \, \exp[-\beta[\mathcal{H}(p',r)]3N/L]}{\int dp'^N dr^N \, \exp[-\beta[\mathcal{H}(p',r)]3(N+1)/L]} \right\}}$$

$$= \frac{\int dp'^N dr^N \, A(p/s, r) \exp\left[-\beta \mathcal{H}(p',r)3N/L\right]}{\int dp'^N dr^N \, \exp[-\beta[\mathcal{H}(p',r)]3N/L]}$$

$$= \langle A(p/s, r) \rangle_{NVT}. \qquad (6.1.18)$$

In the last step we have assumed that $L = 3N$. Therefore, if we use a sampling scheme based on equal time steps in real time, we have to use a different value for L.

From the Hamiltonian (6.1.6), we can derive the equations of motion for the virtual variables p, r, and t:

$$\frac{dr_i}{dt} = \frac{\partial \mathcal{H}_{Nose}}{\partial p_i} = p_i/(m_i s^2)$$
$$\frac{dp_i}{dt} = -\frac{\partial \mathcal{H}_{Nose}}{\partial r_i} = -\frac{\partial \mathcal{U}(r^N)}{\partial r_i}$$
$$\frac{ds}{dt} = \frac{\partial \mathcal{H}_{Nose}}{\partial p_s} = p_s/Q$$
$$\frac{dp_s}{dt} = -\frac{\partial \mathcal{H}_{Nose}}{\partial s} = \left(\sum_i p_i^2/(m_i s^2) - \frac{L}{\beta} \right)/s.$$

In terms of the real variables, these equations of motion can be written as

$$\frac{dr'_i}{dt'} = s\frac{dr_i}{dt} = p_i/(m_i s) = p'_i/m_i \qquad (6.1.19)$$
$$\frac{dp'_i}{dt'} = s\frac{dp_i/s}{dt} = \frac{dp_i}{dt} - \frac{1}{s}p_i\frac{ds}{dt} \qquad (6.1.20)$$
$$= -\frac{\partial \mathcal{U}(r'^N)}{\partial r'_i} - (s'p'_s/Q)p'_i$$
$$\frac{1}{s}\frac{ds'}{dt'} = \frac{s}{s}\frac{ds}{dt} = s'p'_s/Q \qquad (6.1.21)$$
$$\frac{d(s'p'_s/Q)}{dt'} = \frac{s}{Q}\frac{dp_s}{dt}$$
$$= \left(\sum_i p'^2_i/m_i - \frac{L}{\beta} \right)/Q. \qquad (6.1.22)$$

For these equations of motion, the following quantity is conserved:

$$H'_{Nose} = \sum_{i=1}^N \frac{p'^2_i}{2m_i} + \mathcal{U}(r'^N) + \frac{s'^2 p'^2_s}{2Q} + L\frac{\ln s'}{\beta}. \qquad (6.1.23)$$

It should be stressed, however, that this H'_{Nose} is not a Hamiltonian, since the equations of motion cannot be derived from it.

Implementation

In the previous section we showed how the introduction of an additional dynamical variable (s) in the Lagrangian can be used to perform MD simulations subject to a constraint (in this case, constant temperature). We stress

once again that the importance of such extended Lagrangian techniques transcends the specific application. In addition, the problems encountered in the numerical implementation of the Nosé scheme are representative of a wider class of algorithms (namely, those where forces depend explicitly on velocities). It is for this reason that we discuss the numerical implementation of the Nosé thermostat in some detail (see also Appendix E.2).

The Nosé equations of motion can be written in terms of virtual variables or real variables. In a simulation it is not convenient to work with fluctuating time intervals. Therefore the real-variable formulation is recommended. Hoover [132] has shown that the equations derived by Nosé can be further simplified [133]. In equations (6.1.20), (6.1.21), and (6.1.22), the variables s', p_s', and Q occur only as $s'p_s'/Q$. To simplify these equations, we can introduce the thermodynamic friction coefficient $\xi = s'p_s'/Q$. The equations of motion then become (dropping the primes and using dots to denote time derivatives)

$$\dot{r}_i = p_i/m_i \tag{6.1.24}$$

$$\dot{p}_i = -\frac{\partial \mathcal{U}(r^N)}{\partial r_i} - \xi p_i \tag{6.1.25}$$

$$\dot{\xi} = \left(\sum_i p_i^2/m_i - \frac{L}{\beta} \right) /Q \tag{6.1.26}$$

$$\dot{s}/s = \frac{d \ln s}{dt} = \xi. \tag{6.1.27}$$

Note that the last equation, in fact, is redundant, since equations (6.1.24)–(6.1.26) form a closed set. However, if we solve the equations of motion for s as well, we can use equation (6.1.23) as a diagnostic tool, since H′ has to be conserved during the simulation. In terms of the variables used in equations (6.1.24)–(6.1.27), H reads

$$H_{Nose} = \sum_{i=1}^{N} \frac{p_i^2}{2m_i} + \mathcal{U}(r^N) + \frac{\xi^2 Q}{2} + L\frac{\ln s}{\beta}. \tag{6.1.28}$$

As we use the real-variable formulation in this set of equations, we have to take $L = 3N$.

An important implication of the Nosé equations is that in the Lagrangian (6.1.3) a logarithmic term (ln s) is needed to have the correct scaling of time. Any other scheme that does not have such a logarithmic term will fail to describe the canonical ensemble correctly.

An important result obtained by Hoover [132] is that the equations of motion (6.1.24)–(6.1.26) are unique, in the sense that other equations of the same form cannot lead to a canonical distribution. In Appendix E.2 we discuss an efficient way of implementing the Nosé-Hoover scheme.

The equations of motion of the Nosé-Hoover scheme cannot be derived from a Hamiltonian. This implies that one cannot use the standard methods (see Appendix A) to make the connection of the dynamics generated by solving these equations of motion with Statistical Mechanics. In Appendix B we discuss how one can analyze such non-Hamiltonian dynamics. The result of this analysis is that the conventional Nosé-Hoover algorithm only generates the correct distribution if there is a *single* constant of motion. Normally, the total energy defined by H_{Nose}, see equation (6.1.28), is always conserved. This implies that one should not have any other conserved quantity. In most conventional simulations this is the case if the momentum is not conserved, for example, if their is an external force; i.e., the sum of the forces $\sum_i F_i \neq 0$. If we simulate a system without external forces, $\sum_i F_i = 0$, which implies we have an additional conservation law, the Nosé-Hoover scheme is still correct provided that the center of mass remains fixed. This condition can be fulfilled easily if we ensure that during the equilibration the velocity of the center of mass is set to 0. If we simulate a system using no external field and in which the center of mass is not fixed or if we have more than one conservation law, we have to use Nosé-Hoover chains to obtain the correct canonical distribution. This method will be discussed in section 6.1.3.

Application

We illustrate some of the points discussed above in a Nosé-Hoover simulation of the Lennard-Jones fluid.
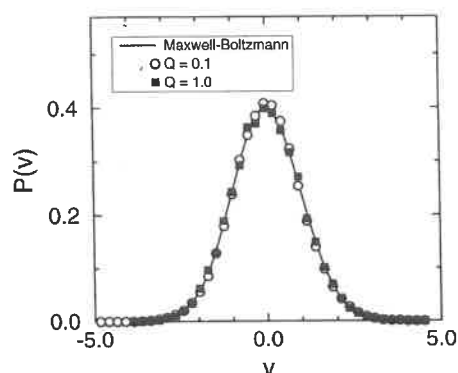
Case Study 11 (Lennard-Jones: Nosé-Hoover Thermostat)

As in Case Study 10, we start by showing that the Nosé-Hoover method reproduces the behavior of a system at constant NVT. In Figure 6.4 we compare the velocity distribution generated by the Nosé-Hoover thermostat with the correct Maxwell-Boltzmann distribution for the same temperature (6.1.1). The figure illustrates that the velocity distribution indeed is independent of the value chosen for the coupling constant Q.

It is instructive to see how the system reacts to a sudden increase in the imposed temperature. Figure 6.5 shows the evolution of the kinetic temperature of the system. After 12,000 time steps the imposed temperature is suddenly increased from T = 1 to T = 1.5. The figure illustrates the role of the coupling constant Q. A small value of Q corresponds to a low inertia of the heat bath and leads to rapid temperature fluctuations. A large value of Q leads to a slow, ringing response to the temperature jump.

Next, we consider the effect of the Nosé-Hoover coupling constant Q on the diffusion coefficient. As can be seen in Figure 6.6, the effect is much smaller than in Andersen's method. However, it would be wrong to conclude that the diffusion coefficient is independent of Q. The Nosé-Hoover method simply provides a way to keep the temperature constant more gentle than

Figure 6.4: Velocity distribution in a Lennard-Jones fluid (T = 1.0, ρ = 0.75, and N = 256). The solid line is the Maxwell-Boltzmann distribution (6.1.1) the symbols were obtained in a simulation using the Nosé-Hoover thermostat.
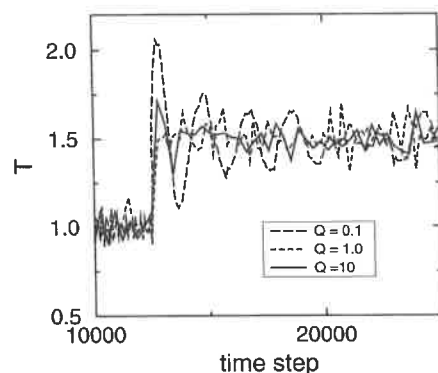
Figure 6.5: Response of the system to a sudden increase of the imposed temperature. The various lines show the actual temperature of the system (a Lennard-Jones fluid ρ = 0.75, and N = 256) as a function of the number of time steps for various values of the Nosé-Hoover coupling constant Q.

Andersen's method where particles suddenly get new, random velocities. For the calculations of transport properties, we prefer simple N,V,E simulations.
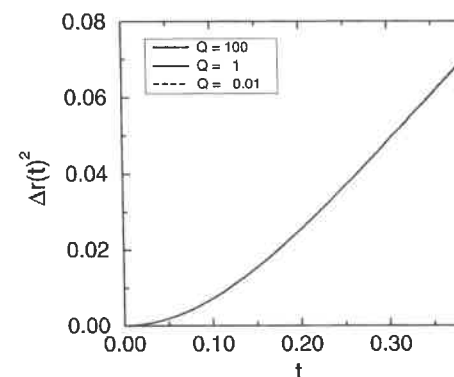
Figure 6.6: Effect of the coupling constant Q on the mean-squared displacement for a Lennard-Jones fluid (T = 1.0, ρ = 0.75, and N = 256).

6.1.3 Nosé-Hoover Chains

In the preceding examples, we have applied the Andersen and Nosé-Hoover thermostats to the Lennard-Jones fluid. For the Nosé-Hoover thermostat we have shown that for a system in which there are no external forces and the center of mass remains fixed, a canonical distribution will be generated. However, even though for systems with external forces the Nosé-Hoover thermostat generates the desired distribution, there can be exceptional cases in which we do not find the expected behavior. To illustrate this, we consider a particularly pathological case, namely, the one-dimensional harmonic oscillator.

Case Study 12 (Harmonic Oscillator (I))
As the equations of motion of the harmonic oscillator can be solved analytically, this model system is often used to test algorithms. However, the harmonic oscillator is also a rather atypical dynamical system. This will show up clearly when we apply our thermostating algorithms to this simple model system.

The potential energy function of the harmonic oscillator is

$$u(r) = \frac{1}{2}r^2 .$$

The Newtonian equations of motion are

$$\dot{r} = v$$
$$\dot{v} = -r .$$
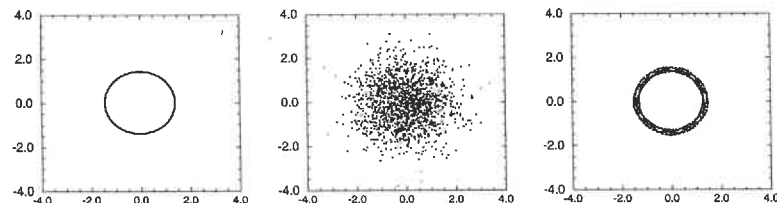
Figure 6.7: Trajectories of the harmonic oscillator: (from left to right) in the microcanonical ensemble, using the Andersen method, and using the Nosé-Hoover method. The y axis is the velocity and the x axis is the position.

If we solve the equations of motion of the harmonic oscillator for a given set of initial conditions, we can trace the trajectory of the system in phase space. Figure 6.7 shows a typical phase space trajectory of the harmonic oscillator, in a closed loop, which is characteristic of periodic motion. It is straight-forward to simulate a harmonic oscillator at constant temperature using the Andersen thermostat (see section 6.1.1). A trajectory is shown in Figure 6.7. In this case the trajectories are points that are not connected by lines. This is due to the stochastic collisions with the bath. In this example, we allowed the oscillator to interact with the heat bath at each time step. As a result, the phase space density is a collection of discrete points. The resulting veloc-ity distribution is Gaussian by construction; also for the positions we find a Gaussian distribution.

We can also perform a constant-temperature Nosé-Hoover simulation us-ing the algorithm described in Appendix E.2. A typical trajectory of the har-monic oscillator generated with the Nosé-Hoover scheme is shown in Fig-ure 6.7. The most striking feature of Figure 6.7 is that, unlike the Andersen scheme, the Nosé-Hoover method does not yield a canonical distribution in phase space. Even for very long simulations, the entire trajectory would lie in the same ribbon shown in Figure 6.7. Moreover, this band of trajectories depends on the initial configuration. This nonergodic behavior of the Nosé-Hoover algorithm was first discovered by Hoover [131]. Toxvaerd and Olson have shown that similar effects can also be observed in the simulation of a realistic model for butane [134]. The reason why we do not find a canonical distribution is that conservation of energy is not the only conservation law. Tuckerman *et al.* [135] have shown that an additional conservation law ex-ists. In Appendix B.2.1 we show that in the presence of such an additional conservation law the algorithm does not generate the desired distribution.

In the previous section it is argued that the Nosé-Hoover algorithm only generates a correct canonical distribution for molecular systems in which

there in only one conserved quantity or if there are no external forces and the center of mass remains fixed. The last condition can be obeyed in most prac-tical systems by initializing the system with a zero center-of-mass velocity. However, if one is interested in simulating more general systems one cannot rely on the simple Nosé-Hoover algorithm. At this point it is important to note that the Andersen thermostat does not suffer from such problems, but its dynamics is less realistic.

To alleviate the restriction for the Nosé-Hoover thermostat, Martyna *et al.* [136] proposed a scheme in which the Nosé-Hoover thermostat is coupled to another thermostat or, if necessary, to a whole chain of thermostats. As we show in Appendix B.2.2 these chains take into account additional con-servation laws. In [136] it is shown that this generalization of the original Nosé-Hoover method still generates a canonical distribution (provided that it is ergodic).

The equations of motion for a system of N particles coupled with M Nosé-Hoover chains are given (in real variables, hence L = 3N) by

$$\dot{r}_i = \frac{p_i}{m_i} \tag{6.1.29}$$

$$\dot{p}_i = F_i - \frac{p_{\xi_1}}{Q_1}p_i \tag{6.1.30}$$

$$\dot{\xi}_k = \frac{p_{\xi_k}}{Q_k} \qquad k = 1, \ldots, M \tag{6.1.31}$$

$$\dot{p}_{\xi_1} = \left(\sum_i \frac{p_i^2}{m_i} - Lk_BT \right) - \frac{p_{\xi_2}}{Q_2}p_{\xi_1} \tag{6.1.32}$$

$$\dot{p}_{\xi_k} = \left[\frac{p_{\xi_{k-1}}^2}{Q_{k-1}} - k_BT \right] - \frac{p_{\xi_{k+1}}}{Q_{k+1}}p_{\xi_k} \tag{6.1.33}$$

$$\dot{p}_{\xi_M} = \left[\frac{p_{\xi_{M-1}}^2}{Q_{M-1}} - k_BT \right]. \tag{6.1.34}$$

For these equations of motion the conserved energy is

$$H_{NHC} = \mathcal{H}(r, p) + \sum_{k=1}^{M} \frac{p_{\xi_k}^2}{2Q_k} + Lk_BT\xi_1 + \sum_{k=2}^{M} k_BT\xi_k. \tag{6.1.35}$$

We can use this conserved quantity to check the integration scheme. It is im-portant to note that the additional M − 1 equations of motion form a simple one-dimensional chain and therefore are relatively simple to implement. In Appendix E.2, we describe an algorithm for a system with a Nosé-Hoover chain thermostat.
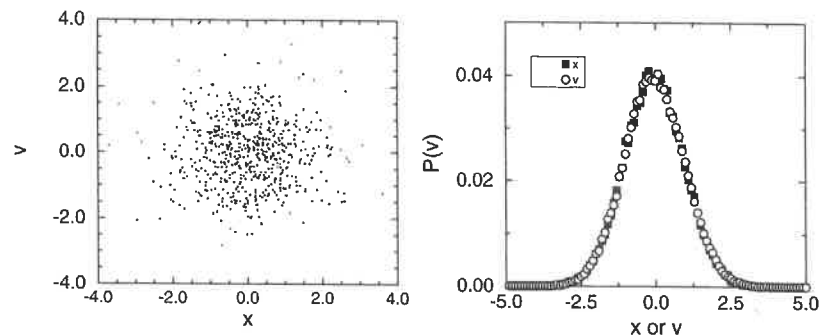
Figure 6.8: Test of the phase space trajectory of a harmonic oscillator, coupled to a Nosé-Hoover chain thermostat. The left-hand side of the figure shows part of a trajectory: the dots correspond to consecutive points separated by 10,000 time steps. The right-hand side shows the distributions of velocity and position. Due to our choice of units, both distributions should be Gaussians of equal width.

Case Study 13 (Harmonic Oscillator (II))
The harmonic oscillator is the obvious model system on which we test the Nosé-Hoover chain thermostat. If we use a chain of two coupling parameters, the equations of motion are

$$
\begin{aligned}
\dot{r} &= v \\
\dot{v} &= -r - \xi_1 v \\
\dot{\xi_1} &= \frac{v^2 - T}{Q_1} - \xi_1 \xi_2 \\
\dot{\xi_2} &= \frac{Q_1 \xi_1^2 - T}{Q_2}.
\end{aligned}
$$

A typical trajectory generated with the Nosé-Hoover chains is shown in Figure 6.8. The distribution of the velocity and position of the oscillator are also shown in Figure 6.8. Comparison with the results obtained using the Andersen thermostat (see Case Study 12) shows that the Nosé-Hoover chains do generate a canonical distribution, even for the harmonic oscillator.

6.2 Molecular Dynamics at Constant Pressure

Most experiments are performed at constant pressure instead of constant volume. If one is interested in simulating the effect of, for example, the com-

position of the solvent on the properties of a system one has to adjust the volume of an N,V,T simulation to ensure that the pressure remains constant. For such a system it is therefore much more convenient to simulate at constant pressure. To simulate at constant pressure in a Molecular Dynamics simulation the volume is considered as a dynamical variable that changes during the simulation.

In Chapter 5 we have seen that one can perform Monte Carlo simulations at constant pressure by changing the volume of the simulation box. Here we consider the equivalent for a Molecular Dynamics simulation. Similar to the Monte Carlo case, this is an excellent method for homogeneous fluids. For inhomogeneous systems, however, one may need to change the shape of the simulation box as well [102,103].

In Appendix B we have shown that the correct thermostating of a Molecular Dynamics simulation has many subtleties related to the conservation laws and whether a simulation is performed with a fixed center of mass. Similar problems arise with the isothermal-isobaric ensemble. The earlier scheme of Hoover [132] can only approximate the desired distribution [137]. Since the scheme of Martyna *et al.* does give the desired distribution, we focus on this scheme. All these schemes are based on the extended ensemble approach pioneered by Andersen [104].

The equations of motion proposed by Martyna *et al.* [138] for the positions and the momenta are

$$
\dot{r}_i = \frac{p_i}{m_i} + \frac{p_\epsilon}{W} r_i \tag{6.2.1}
$$

$$
\dot{p}_i = F_i - \left(1 + \frac{d}{dN}\right) \frac{p_\epsilon}{W} p_i - \frac{p_{\xi_1}}{Q_1} p_i, \tag{6.2.2}
$$

where N is the number of particles. In these equations of motion we recognize a thermostat that is introduced via the variables ξ_1, p_{ξ_1}, and Q_1, similar to the N,V,T version of the Nosé-Hoover chain algorithm. A barostat is introduced via the variables ϵ, p_ϵ, and W. ϵ is defined as the logarithm of the volume V of the system

$$
\epsilon = \ln(V/V(0)),
$$

where $V(0)$ is the volume at $t = 0$, W is the mass parameter associated to ϵ, and p_ϵ is the momentum conjugate to ϵ.

The equations of motion (6.2.1) and (6.2.2) are complemented with an equation of motion for the volume, which reads in d dimensions

$$
\dot{V} = \frac{dVp_\epsilon}{W} \tag{6.2.3}
$$

$$
\dot{p}_\epsilon = dV(P_{int} - P_{ext}) + \frac{1}{N} \sum_{i=1}^{N} \frac{p_i^2}{m_i} - \frac{p_{\xi_1}}{Q_1} p_\epsilon. \tag{6.2.4}
$$

In these equations P_{ext} is the external pressure, which is imposed (like the temperature). P_{int} is the internal pressure, which can be calculated during the simulation

$$P_{int} = \frac{1}{dV} \left[\sum_{i=1}^{N} \left(\frac{p_i^2}{m_i} + r_i \cdot F_i \right) - dV \frac{\partial U(V)}{\partial V} \right],$$

where U is the potential. This equation differs from the conventional virial equation for a constant-volume simulation.

The equations of the chain of length M are[2]

$$\dot{\xi}_k = \frac{p_{\xi_k}}{Q_k} \qquad \text{for } k = 1, \ldots, M \qquad (6.2.5)$$

$$\dot{p}_{\xi_1} = \sum_{i=1}^{N} \frac{p_i^2}{m_i} + \frac{p_\epsilon^2}{W} - (dN+1)k_B T - \frac{p_{\xi_2}}{Q_2} p_{\xi_1} \qquad (6.2.6)$$

$$\dot{p}_{\xi_k} = \frac{p_{\xi_{k-1}}^2}{Q_{k-1}} - k_B T - \frac{p_{\xi_{k+1}}}{Q_{k+1}} p_{\xi_k} \qquad \text{for } k = 2, \ldots, M-1 \quad (6.2.7)$$

$$\dot{p}_{\xi_M} = \frac{p_{\xi_{M-1}}^2}{Q_{M-1}} - k_B T. \qquad (6.2.8)$$

The conserved quantity for these equations of motion is

$$H_{N, P_{ext}, T} = \mathcal{H}(\mathbf{p}, \mathbf{r}) + \frac{p_\epsilon^2}{W} + \sum_{k=1}^{M} \frac{p_{\xi_k}^2}{Q_k} + (dN+1)k_B T \xi_1$$

$$+ k_B T \sum_{k=1}^{M} \xi_k + P_{ext} V. \qquad (6.2.9)$$

In Appendix B.3 we demonstrate that this method indeed generates the correct distribution. The implementation of this algorithm is described in Appendix E.2.2.

6.3   Questions and Exercises

Question 14 (Andersen Thermostat)

1. *Why is it that the static properties calculated by NVT-MD using the Andersen thermostat do not depend on ν?*

---

[2]Here we give the equations of motion in which the particles and the barostat are coupled to the same Nosé-Hoover chain. The more general case is to couple the particle and the barostat to two different thermostats. The advantage of having two different chains is that they can be optimized to the different time scales associated with temperature and volume fluctuations. Since in practice these times scales can be very different it is advised to use two different chains. The equations of motion can be found in Ref. [137].

2. *Why does the diffusivity decrease with increasing ν?*

Question 15 (Nosé-Hoover Thermostat)

1. *Explain when do we have to use $g = 3N + 1$ and $g = 3N$ in the Nosé-Hoover thermostat.*

2. *Instead of a single Nosé-Hoover thermostat, one can also use a chain of thermostats. Does this lead to a significant increase of the total CPU time for the simulation of a large system?*

3. *Another widely used thermostat is the "temperature coupling" of Berendsen et al. [139]. This method, however, does not generate the canonical ensemble exactly. In this algorithm, the temperature of the system is controlled by scaling the velocities to every time step with a factor λ*

$$\lambda = \left[1 + \frac{\Delta t}{\tau_T} \left(\frac{T_0}{T} - 1 \right) \right]^{\frac{1}{2}}, \qquad (6.3.1)$$

in which T_0 is the desired temperature, T is the actual temperature, Δt is the time step of the integration algorithm and τ_T is a constant.

- *Show that this scaling is equivalent to a temperature coupling of the system with a heat bath at $T = T_0$*

$$J = \alpha (T_0 - T), \qquad (6.3.2)$$

in which J is the heat flux and α is the heat transfer coefficient.

- *What is the relation between α and τ_T?*

Exercise 13 (Barrier Crossing (Part 1))

Consider the movement of a single particle that moves on a 1D potential energy surface with the following functional form:

$$U(x) = \begin{cases} \epsilon B x^2 & x < 0 \\ \epsilon (1 - \cos(2\pi x)) & 0 \leq x \leq 1. \\ \epsilon B (x-1)^2 & x > 1 \end{cases}$$

The energy, force, and the derivative of the force are continuous functions of the position x and $\epsilon > 0$.

1. Derive an expression for B. Make a sketch of the potential energy landscape.

2. You can find a program on the book's website that integrates the equation of motion of the particle starting at $x(t=0) = 0$ using several methods:

(a) No thermostat (NVE ensemble). What do you expect the phase space trajectories to look like?

(b) Andersen thermostat. In this method, the velocity of the particle is coupled to a stochastic heat bath, which leads to a canonical distribution.

(c) A Nosé-Hoover chain. In this method, the motion of the particle is coupled to a chain of thermostats. The equations of motion are integrated using an explicit time-reversible algorithm that might look a little bit complicated at first sight (see Appendix E.2.1), see *integrate_res.f*. One can prove that this method yields a canonical distribution provided that the system is ergodic.

(d) No molecular dynamics, but a simple Monte Carlo scheme.

The Andersen thermostat and the NVE integration algorithm are not implemented yet, so you will have to do this yourself (see *integrate_nve.f* and *integrate_and.f*). Try to use all methods for a low temperature, $T = 0.05$, for which the system behaves like a harmonic oscillator. Pay special attention to the following:

(a) Why does the distribution of the MC scheme look so much different at low temperatures?

(b) Why does the phase space distribution of the NVE scheme look like a circle (or ellipse)?

(c) Compare the phase space distributions of the Nosé-Hoover chain method with distribution generated by the Andersen thermostat. How long should the Nosé-Hoover chain be to generate a canonical distribution?

3. Investigate at which temperature the probability that the particle crosses the energy barrier becomes nonnegligible.

4. Another widely used algorithm is the "temperature coupling" of Berendsen *et al.* [139]. This method does not produce a true canonical ensemble. In this algorithm, the temperature of the system is controlled by scaling the velocities every time step with a factor λ

$$\lambda = \left[1 + \frac{\Delta t}{\tau_T}\left(\frac{T_0}{T} - 1\right)\right]^{\frac{1}{2}}, \qquad (6.3.3)$$

in which T_0 is the desired temperature, T is the actual temperature, Δt is the time step of the integration algorithm, and τ_T is a constant. The temperature coupling algorithm can be used in combination with a

Leap-Frog Algorithm

$$v\left(t + \frac{\Delta t}{2}\right) = \lambda\left(t - \frac{\Delta t}{2}\right) \times \left(v\left(t - \frac{\Delta t}{2}\right) + \frac{F(t)}{m}\Delta t\right)$$

$$x(t + \Delta t) = x(t) + v\left(t + \frac{\Delta t}{2}\right)\Delta t. \qquad (6.3.4)$$

Compare the distributions of the Berendsen *et al.* temperature bath with the canonical distributions.

5. Modify the program in such a way that the potential energy function

$$U = \epsilon[1 - \cos(2\pi x)] \qquad (6.3.5)$$

is used. Calculate the diffusion coefficient as a function of the temperature. Why is it impossible to calculate the diffusivity at low temperatures using ordinary molecular dynamics? Why is the diffusion coefficient obtained by using the Andersen thermostat a function of the collision frequency?